PROTEINS
STRUCTURE ■ FUNCTION ■ BIOINFORMATICS

Structural modeling and molecular dynamics simulation of the actin filament

Thomas Splettstoesser,[1] Kenneth C. Holmes,[2] Frank Noé,[3] and Jeremy C. Smith[1,4]*

[1] Interdisciplinary Center for Scientific Computing, University of Heidelberg, 69120 Heidelberg, Germany
[2] Max Planck Institut für Medizinische Forschung, 69120 Heidelberg, Germany
[3] DFG Research Center Matheon, FU Berlin, Arnimallee 6, 14159 Berlin, Germany
[4] Center for Molecular Biophysics, Oak Ridge National Lab, University of Tennessee/ORNL, Oak Ridge, Tennessee 37831

ABSTRACT

Actin is a major structural protein of the eukaryotic cytoskeleton and enables cell motility. Here, we present a model of the actin filament (F-actin) that not only incorporates the global structure of the recently published model by Oda *et al.* but also conserves internal stereochemistry. A comparison is made using molecular dynamics simulation of the model with other recent F-actin models. A number of structural determents such as the protomer propeller angle, the number of hydrogen bonds, and the structural variation among the protomers are analyzed. The MD comparison is found to reflect the evolution in quality of actin models over the last 6 years. In addition, simulations of the model are carried out in states with both ADP or ATP bound and local hydrogen-bonding differences characterized.

Proteins 2011; 79:2033–2043.

Key words: actin; filament; molecular dynamics; model; conformational change.

INTRODUCTION

Actin, a highly conserved structural protein found in virtually all eukaryotic cells, exists in two forms: monomeric G-actin and the filament, F-actin. F-actin is formed by the ATP-dependent assembly of G-actin monomers, the nucleotide binding site lying in the cleft between the two domains of the G-actin monomer.[1] Actin has been a major target of structural studies for decades.[2–4] However, owing to the difficulties involved in crystallizing the filament, the atomic-detail structure of F-actin is still unknown.

X-ray fiber diffraction experiments of the filament suggesting a helical conformation were carried out as early as 1947,[5,6] and this was confirmed in 1963 by electron microscopy (EM).[7] Subsequent cryo-EM studies of actin in the 1980s reached resolutions of 20–30 Å.[8] In 1990, the first atomic-detail structure of monomeric G-actin was determined by X-ray crystallography.[9] This achievement allowed the first high-resolution filament model to be proposed.[10] In this and subsequent work,[11,12] a helix of G-actin monomers was fitted to the X-ray fiber diffraction pattern of oriented actin gels. The quality of the fit thus obtained suggests that the difference in conformation between an actin molecule in its monomeric form and in the filament is relatively small. However, the resolution of the fiber diffraction patterns was only about 6–8 Å and thus the refinement underdetermined.[11] In subsequent years new filament models were proposed using different approaches of optimizing the refinement.[13–15] In 2009 Oda *et al.* were able to obtain resolutions of up to 6 Å, currently the highest reported.[12] Global properties of the helical actin filament, such as diameter of the fibril, helix parameters, and orientation of the actin protomers in the filament have now been reliably determined[16] and are incorporated in the recent model of Oda *et al.*, which we label "Oda 2009."

ATP hydrolysis drives the polymerization and depolymerization cycle of actin. The nature of the actin-bound nucleotide, that is, ADP or ATP, is a key determinant of the conformation of the filament. Experimental studies indicate that release of γ-phosphate, following ATP hydrolysis in the filament, alters properties of F-actin, such as the persistence length and the binding affinity of certain proteins associating with the filament.[17,18] However, the conformational transition associated with ATP hydrolysis is not well understood, due in part to the lack of a high-resolution X-ray structure of the actin filament and also because available F-actin models have been derived mostly based on structures of only ADP-F-actin, which is the predominant state of the actin filament.

Additional Supporting Information may be found in the online version of this article.
Grant sponsor: U.S. Department of Energy (Laboratory-Directed Research and Development grant)
*Correspondence to: Jeremy C. Smith, University of Tennessee/ORNL, Center for Molecular Biophysics, One Bethel Valley Road, Oak Ridge National Lab, Oak Ridge, TN 37831. E-mail: smithjc@ornl.gov.
Received 15 November 2010; Revised 19 January 2011; Accepted 28 January 2011
Published online 1 March 2011 in Wiley Online Library (wileyonlinelibrary.com). DOI: 10.1002/prot.23017

Also, conformational events accompanying to the G-to-F-actin transition have been the subject of debate. For example, the "hydrophobic plug" (Gln263-Ser271), a loop with a hydrophobic tip, has been suggested to functionally alter its position on integration of the G-actin monomer into the filament.[10] Furthermore, the conformation of the DNase I-binding loop (Arg39-Lys50), the most flexible part of the G-actin structure, has been hypothesized to be coupled to the nucleotide-binding state.[19]

To clarify questions such as the above further improvements of the F-actin structure are required. In the present work, we propose a model of the actin filament, which we label "Holmes 2010." This model was built using a straightforward approach in which priority was given to keeping the stereochemistry within the actin protomer intact while altering the position of the two actin domains to account for the global conformational change during the G-to-F-actin transition. The low-resolution, global tertiary structure of the new model (defined by the orientation and position of the four subdomains relative to each other) is derived from, and thus similar to, the Oda 2009 model,[12] but in terms of secondary structure and specific interactions, such as in the nucleotide binding site, the new model mostly resembles the G-actin structure[19] on which it is based. The fiber diffraction pattern calculated from the new model matches the experimental pattern.

Furthermore, a comparison is made of the structures and dynamics of Holmes 2010 with other recent models by subjecting them to MD simulation. The models chosen for comparison are Oda 2009 and another,[11] based on a previously obtained diffraction pattern (6–8 Å), which we name "Holmes 2004." The MD comparison is found to reflect the evolution in quality of the actin models over the last 6 years.

Finally, simulations are performed on how the nucleotide (ADP or ATP) affects the conformation of the Holmes 2010 actin filament, with a particular focus on the phenomenon of G-to-F-actin ATPase activation. In agreement with previous studies, we predict the importance of Gln137 for ATP hydrolysis, which in the model, and even more so in the MD simulation, comes into close proximity to the ATP.

METHODS

Holmes 2010 model

The F-actin model proposed here, "Holmes 2010," was constructed starting from the tetramethylrhodamine-labeled G-actin X-ray structure [Protein Data Bank (PDB)[20] entry 1J6Z] of Ref. 19. The global conformational transition accompanying the G-to-F-actin transition is a flattening of the actin molecule by a twist of the two domains relative to each other, as shown in Figure S1 in the Supporting Information. This global conformation of the actin molecule in the filament was later confirmed by Fujii *et al.*[15] Therefore, in our modeling, the two domains of the G-actin monomer were fitted separately (junctions at residues 139–140, 341–342) to the two domains of the Oda 2009 model. The compact α-helical conformation of the DNase-binding loop in PDB 1J6Z is likely an artifact[15,21] and thus was discarded and replaced by the more extended "open loop" coordinates of the Oda 2009 model (residues 35–69). Phalloidin was added in and the coordinates refined against the fiber diffraction data and EM data,[22] weighted in favor of the fiber data. The final radius of gyration is 23.7 Å. Figure S2A in the Supporting Information shows that the diffraction pattern calculated from our "Holmes 2010" F-actin model is consistent with the observed pattern. Coordinates of Holmes 2010 are deposited at http://cmb.ornl.gov/Members/spe/5_actin.pdb/view.

To compare the dynamical properties of the three structural models, MD simulations were performed of a 13-protomer repeat of the actin filament, corresponding to a 180° turn of the helical filament, using 3D periodic boundary conditions and thus creating an infinite filament. For reference, 13 independent molecular dynamics simulations were also carried out using a crystal structure of ADP-bound G-actin (PDB entry 1J6Z[19]).

Simulation models

A summary of the simulation models and system sizes is given in Table I. Interestingly, the Holmes 2004, Oda 2009, and Holmes 2010 structural models all started from the structure of ADP-G-actin, PDB ID 1J6Z[19].

Actin filaments consist of identical actin molecules (protomers). The 1990 filament model of Holmes *et al.*[10] was used to generate the initial organization of the 13 protomers in the filament with a clockwise rotation of 166.2° and translation of 27.5 Å of the protomers along the longitudinal axis.

For the simulations of the Holmes 2010 model with ATP, the ADP coordinates were replaced with the ATP coordinates of the ATP-G-actin structure of PDB 1ATN.[9] The protonation states of the histidine residues were derived by calculating pK values using the H++ webserver.[23] His73 is methylated *in vivo* and in the simulation models and has been shown to be a structural determinant of actin that may be involved in phosphate release.[24]

Molecular dynamics simulations

As well as the tightly bound Mg^{2+} ion in the nucleotide-binding site, several low-affinity binding sites for divalent cations have been observed in crystal structures of G-actin. Occupation of these low-affinity cation binding sites induces polymerization of the actin filament,

Table I
Overview of the Models Studied by MD Simulation

Model	# of actin molecules	Nucleotide	Simulation box (Å)	System size (atoms)	Simulation time (ns)
Filament Simulation					
Holmes 2004[11]	13	ADP	125 × 125 × 358	597,540	30
Oda 2009[12]	13	ADP	125 × 125 × 358	601,443	30
Holmes 2010	13	ADP	125 × 125 × 358	601,413	30
Holmes 2010	13	ATP	125 × 125 × 358	601,476	30
Monomer Simulation					
PDB ID 1J6Z[19]	1	ADP	91 × 91 × 91	77,324	13 × 30

The total simulation time is 440 ns.

suggesting their importance for the integrity of the F-actin polymer.[25] Mg^{2+} ions were placed at G-actin cation-binding sites that have been reported in at least two X-ray structures, derived independently from each other. Mg^{2+} ions were placed at the following three locations: Asp286/Asp288, Glu270/Ser271, and Asp222/Glu224. Physiological concentrations of 139 mM K^+, 12 mM Na^+, and 16 mM Cl^- were used, mimicking cytosolic conditions, and the number of Cl^- ions was adjusted to produce overall charge neutrality.

MD simulations were performed using the NAMD 2.6 package[26] and the CHARMM27 force field.[27] TIP3P water molecules were used to solvate the system.[28] All covalent bonds involving hydrogen atoms were constrained to allow for a 2-fs time step. For short-range electrostatics and van der Waals interactions, a smooth switching function at 8 Å with a cutoff of 10 Å was applied. Long-range electrostatic interactions were computed with the Particle Mesh Ewald procedure[29] and were updated every 4 fs.

The systems were energy minimized for 30,000 steps using the conjugate gradient algorithm with the protein and nucleotide atoms harmonically constrained during the first 20,000 steps. MD simulations were performed in the isothermal-isobaric ensemble (NPT) at 1 atm pressure using the Nosé-Hoover Langevin piston[30] with a decay period of 50 fs. The box dimensions are reported in Table I.

With the harmonic constraints applied, the systems were gradually heated to 300 K over a 30-ps time period. During two subsequent equilibration steps of 100 ps length each, constraints on C_α-atoms were gradually lifted ($1 \rightarrow 0.1 \rightarrow 0$ kcal/mol/Å^2). For each simulation 30 ns of production run was carried out following the heating and equilibration periods.

Analysis

Most properties were assessed on the level of the protomer structure of actin and then averaged over the 13 protomers in the filament. Whole-filament comparison of the different simulations with each other is nontrivial when considering basic quantities such as the RMSD. A slight bending of the entire 13-subunit repeat, which does not affect the filament's structural integrity may result in a large increase in RMSD, overshadowing localized structural defects such as unfolding of secondary structure elements that lead to smaller increases in RMSD. Thus, for certain properties, a meaningful comparison among the three models is possible only on the level of the protomer.

Protomer propeller angle

An actin monomer consists of two domains that can be further divided into four subdomains which form a U-shaped structure (Fig. 1B). The dihedral angle between the centers of mass of the four subdomains (excluding the very flexible DNase I binding loop and the hydrophobic plug) is referred to here as the "propeller angle." It has been shown that on integration of actin monomers into the filament the propeller angle is reduced by about 20°, which flattens the structure of the actin molecule.

RMS deviation over protomers

To examine structural variation among the individual protomers in the 13-subunit repeat, an appropriate RMS backbone atom deviation was derived by calculating, at any given time step, the average protomer structure from the 13 actin molecules, and then the RMS deviation from this average protomer structure of each of the 13 actin molecules was calculated and averaged.

Hydrogen-bonding patterns and calculation of average protomer structure

Default CHARMM settings with a distance cutoff of 2.4 Å and no limit of the angle of linearity were used to define the hydrogen bonds. Patterns of hydrogen bonds between the nucleotides and protein are summarized in Tables S1–3 in the Supporting Information. The occupancy of each hydrogen bond over the last 5 ns of the simulation was calculated for each protomer, and averaged over the 13 protomers. In some protomers, a change in position of the nucleotide within the binding pocket changed lead to an atypical hydrogen binding pattern. To calculate meaningful average interactions,

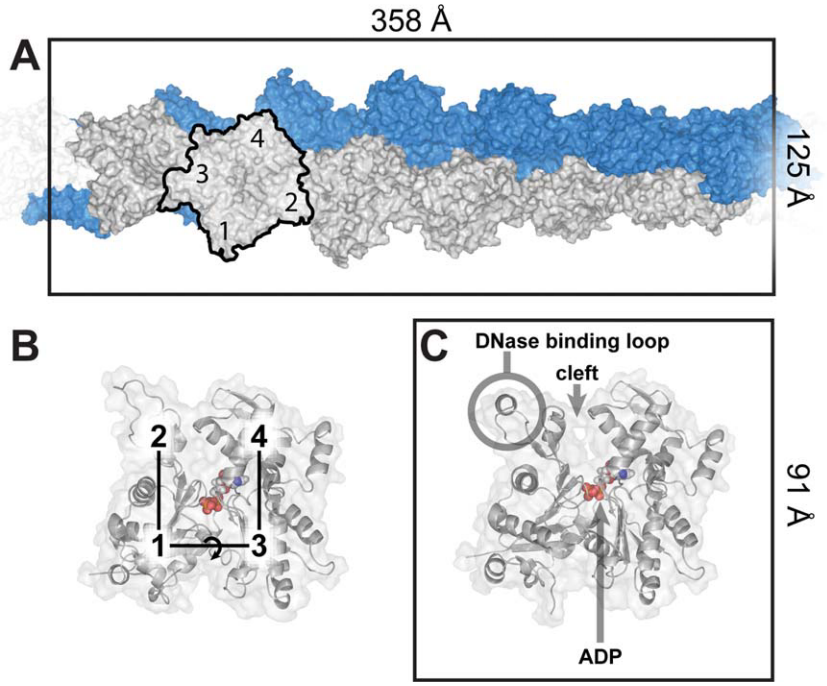

Figure 1

Structures of ADP-bound F- and G-actin. (**A**) The 13-subunit repeat of the Holmes 2010 model is shown in its rectangular MD simulation box. (**B**) Protomer with the four subdomains forming the propeller angle. (**C**) X-ray structure of ADP-bound G-actin used in the monomer simulation (PDB 1J6Z). The DNase binding loop in this G-actin structure (and the Holmes 2004 model) contains an α-helix but adopts an extended conformation without secondary structure in the Oda 2009 and Holmes 2010 models.

hydrogen bonds formed during more than 30% of the simulation time of the last 5 ns were chosen to represent typical nonbonded interactions. Only those protomers with a high occupancy of these >30% interactions were considered for further analysis and used to calculate the average protomer structure.

All molecular images were produced with the program PyMol.[31]

RESULTS

The "Holmes 2010" F-actin filament model was developed, and subsequently, MD simulations of 30-ns length were performed to compare the structure and stability of this model with those of Oda 2009 and Holmes 2004. Simulations of a G-actin crystal structure were also carried out, for comparison with the protomers of the three filament models. To investigate the effects of the nucleotide on the filament structure, a further simulation of the Holmes 2010 model was performed in which ADP was replaced by ATP.

Molecular dynamics simulations

A comparison of the three filament models in the ADP state was performed in which they were subjected to MD simulation. Structural and dynamic properties from MD simulations of the ATP-bound Holmes 2010 F-actin model were also calculated and were found to be very similar to those with ADP bound and thus are not further discussed here but for completeness provided in Figure S3 in the Supporting Information.

In Figure 2A, the backbone root mean-square deviation (RMSD) from the starting structure averaged over the 13 actin molecules in the simulation primary box is shown. The RMSDs of Oda 2009 and Holmes 2010 are similar to that obtained from MD of G-actin, stabilizing around 2.5–3 Å, while the Holmes 2004 protomers reach significantly higher values of ∼4.5 Å, indicating structural instability.

Figure 2B shows the average number of hydrogen bonds within the actin monomers. After an initial equilibration phase, the number of internal hydrogen bonds remains stable for all models. Over the last 5 ns of simulation time numbers for the Holmes 2010 model and G-actin stabilize at ∼300 and ∼295, respectively, significantly higher than Oda 2009, which converges to ∼290. Holmes 2004 is the lowest of the three models at ∼280 to ∼285 hydrogen bonds. In contrast, the Oda 2009 model contains the largest number of hydrogen bonds between the protomers in the filament (Fig. 2C).

The propeller angle formed by the centers of mass of the four subdomains of the actin monomer (see Fig. 1B)

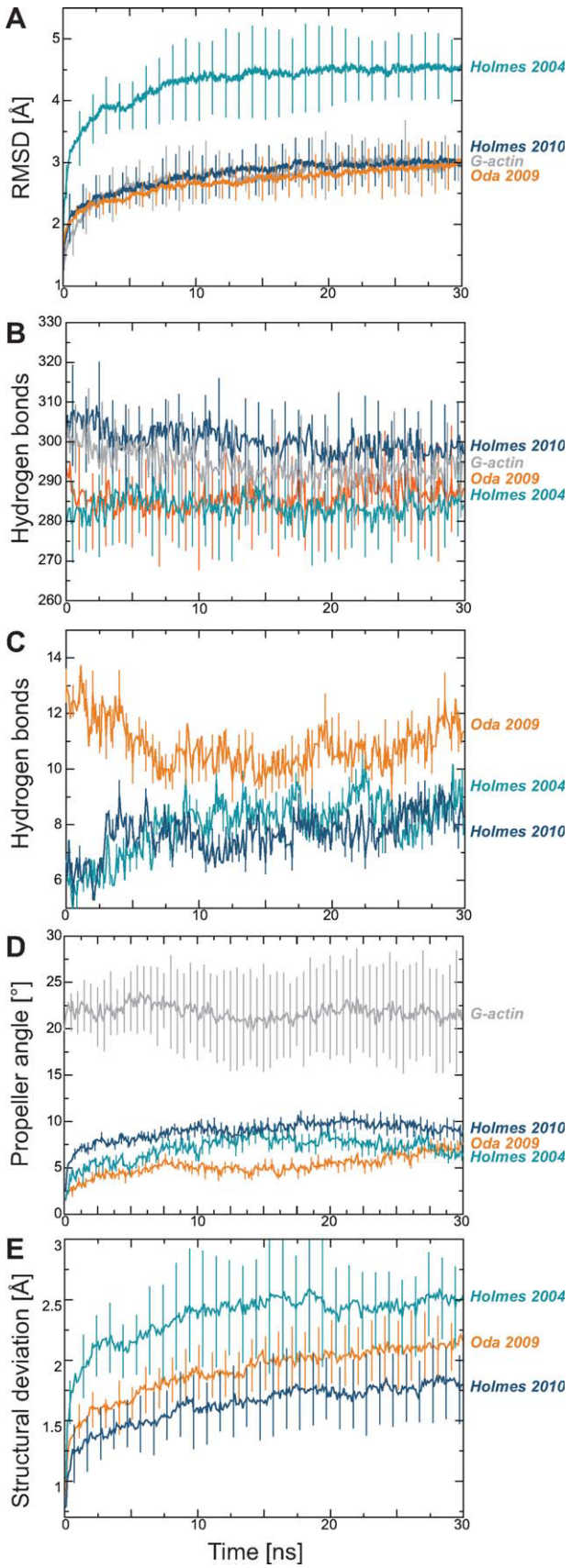

is significantly higher in G-actin (~22°) than in the protomers of F-actin models (~2–3°). As shown in Figure 2D, the low propeller angles, in the range of 2–3°, of the protomers of all three filament models increase significantly on MD simulation to averages ranging from ~7° (Oda) to ~9° (Holmes 2010).

Some studies suggest the existence of a multitude of conformational states of protomers in the filament at any given time. The variation among the conformations of those states has been suggested to be great and extend to the level of the tertiary structure.[32,33] In contrast, other studies point to a well-defined structure of F-actin protomers with little variation.[12,15] In the filament models considered in our study, the protomers within the filament are identical and due to the symmetry of F-actin exposed to the same environment within the filament. Therefore, we consider the structural deviation among the 13 actin molecules in the simulation repeating unit over time as a further indication of stability of a model (Fig. 2E). A certain degree of conformational variation among the protomers is to be expected as a result of thermal fluctuations of the filament around the native state. However, excessive structural variation, especially when accompanied by unfolding of secondary structure elements is likely to arise from the relatively poor quality of the modeled structure that was used to initiate the MD simulation. Here again, the Holmes 2004 model exhibits the highest variation among the protomers and the Holmes 2010 model the lowest. Figure 3 shows the different degrees of conformational deviation among the 13 protomers of each model and the 13 G-actin monomers at the end of the simulation. Some parts of the protomer structure, such as the DNase-binding loop and the variable stretch of residues 227–237 (hereafter referred to as V-stretch), exhibit a high degree of variation in all three models, consistent with the high B-factors of these residues in crystallographic G-actin structures. However, although those parts of the structure with low crystallographic B-factors also exhibit medium and low fluctuations in the Oda 2009 and Holmes 2010 models, respectively, they exhibit high fluctuations in Holmes 2004 pointing to the low structural stability of that model.

Figure 4A compares the backbone per-residue RMS fluctuations of the MD simulations of G-actin and the three models. The DNase binding loop (residues 39–50)

Figure 2

MD time series of structural properties of actin. Each plot represents the average over the 13 actin molecules in the ADP-state. (**A**) Backbone RMSD from starting structure. (**B**) Number of protein hydrogen bonds within an actin molecule. (**C**) Number of hydrogen bonds between a protomer and its two unique interfaces with neighboring protomers (same strand and opposite strand) toward the barbed end of the filament. (**D**) Propeller angle of the centers of mass of the four subdomains of the actin molecule. (**E**) Structural deviation of 13 actin protomers from each other.

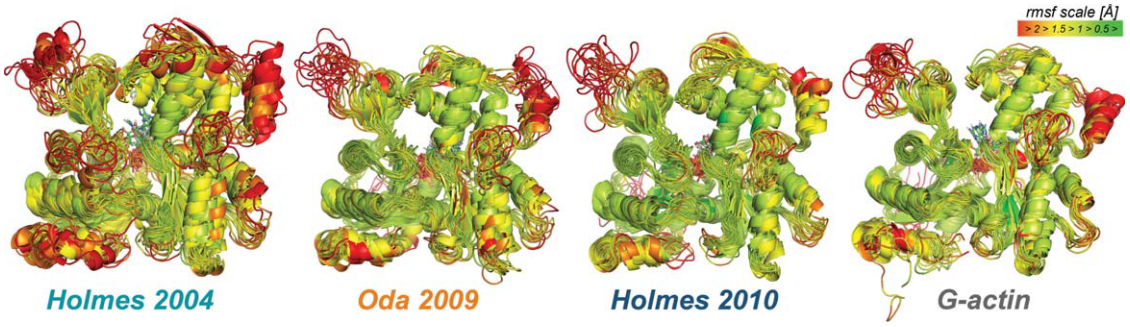

Figure 3

Superposition of the 13 protomer structures after 30 ns of MD simulation by a mass-weighted RMSD fit of the protein backbone. The structures are color-coded by RMS fluctuation per residue over the entire simulation time, where very flexible residues are shown in red and residues with little fluctuation of their position in green.

and residues 220–250 are highly mobile parts of the protein. On average, the fluctuations of the Holmes 2004 simulations are the highest and those of Holmes 2010 the lowest, the latter again being similar to G-actin.

Five segments in which the secondary structures in the simulations of the models are significantly different are highlighted in Figure 4C. The conformation of the DNase-binding loop has been hypothesized to be coupled to the nucleotide state of actin.[19] This loop is disordered in all of the over 40 G-actin crystal structures resolved, with the exception of a tetramethylrhodamine-labeled ADP-bound G-actin structure in which it is an α-helix.[19] It has been suggested that a change of conformation of the loop might explain the different association rates of the ADP- and ATP-bound G-actin to the filament,[19] and also that the α-helix may contribute to the higher flexibility of ADP-F-actin relative to the ATP-bound form.[34] A recent simulation study suggested that the α-helix conformation may be favored only in F-actin.[35] However, these hypotheses have been contested, and it has been suggested that the helix is an artifact of crystallization.[21] Several subsequent studies found no relation between the nucleotide state and the conformation of the DNase-binding loop in G-actin.[36,37] Among the three models considered here, only Holmes 2004 has a DNase-binding loop in α-helical conformation, and this was found to unfold entirely in 6 of the 13 protomers (and, as shown in Fig. 3, in all but one simulation of monomeric G-actin). In the other two models, the loop explores disordered loop conformations throughout the simulations.

The W-loop (residues 165–170), to which WH2-domain containing proteins bind, forms a β-hairpin in the simulations of both Holmes 2004 and Holmes 2010 but a bend in the Oda 2009 MD. The solvent-exposed V-stretch (residues 227–237) includes part of an α-helix and exhibits high RMS fluctuations in the simulations. In most of the Oda-simulation protomers, the helix partially unfolds. In the Holmes 2004 simulation, the helix remains mostly intact but its position varies among the 13 protomers.

The conformation of the "hydrophobic plug" (Gln263-Ser271) in the Holmes 2004 model differs from that in the two newer filament models. In 1990, Holmes *et al.* suggested that this loop may alter its position on integration of the G-actin monomer into the filament by detaching from the surface of the actin molecule and extending into a hydrophobic pocket in the opposing strand, thus, stabilizing the filament. However, later research suggested that the radius of gyration of the earlier actin filament models (such as Holmes 2004; ∼24.8 Å), and thus the distance between the two strands of the long-pitched helix, had been overestimated. The radii of gyration of Oda 2009 and Holmes 2010 are 23.7 and 24 Å, respectively, and in the MD both increase slightly, by 0.3 and 0.2 Å, respectively. Because of the closer proximity of the two strands, an extended hydrophobic plug is not required for the stability of the actin filament.[12] However, it has been suggested that conformational fluctuations of the hydrophobic loop are required for filament formation and stability.[38] In the present MD simulations, the hydrophobic plug showed a high degree of structural variation in Holmes 2004 and some variation in the Oda simulation but was highly conserved among the Holmes 2010 protomers. Residues 348–357 form an α-helix (C-helix) that is located near the C-terminus and remains stable in the Oda simulations but unfolds in some protomers of the two Holmes simulations.

Figure S4 in the Supporting Information superimposes the average protomer from the Holmes 2010 MD simulation, the initial Holmes 2010 model, and the G-actin structure from which the model was derived. For this, an average protomer structure was calculated from selected time-averaged protomer structures (see Methods) from the Holmes 2010 simulation and superimposed on the G-actin structure. Five structural differences between the

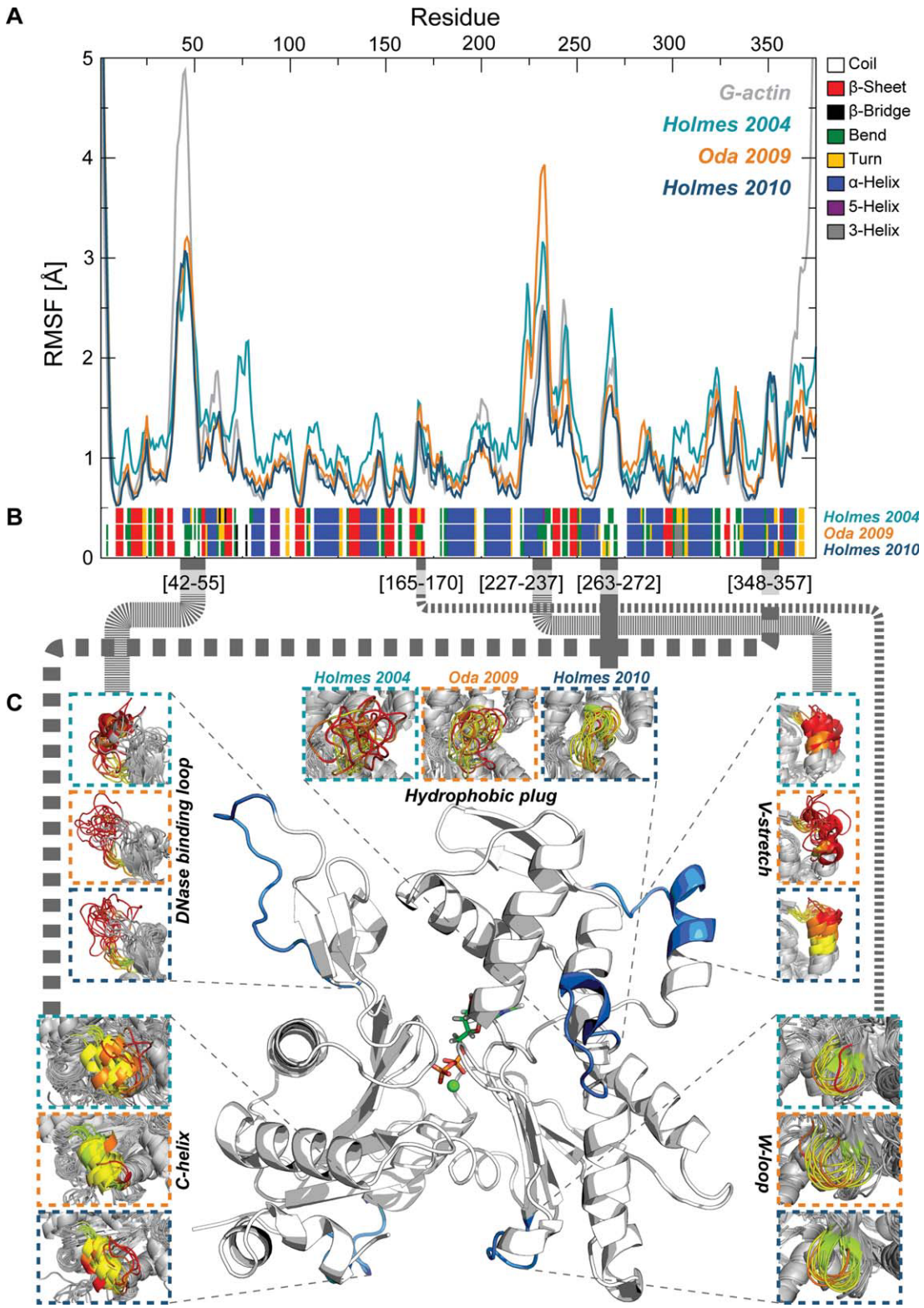

Figure 4

(**A**) Root mean-square fluctuation per residue, averaged over 13 actin molecules. (**B**) Secondary structure profiles of the three filament models, averaged over protomers and over the last 5 ns. For each residue, the most highly occupied state of the 13 profiles is shown. (**C**) Highlighted are five regions of the protomer in which the secondary structure significantly varies among the simulations of the three models: DNase-binding loop (residues 42–55); W-loop (residues 165–170); residues 227–237; hydrophobic plug (residues 263–272); residues 348–357.

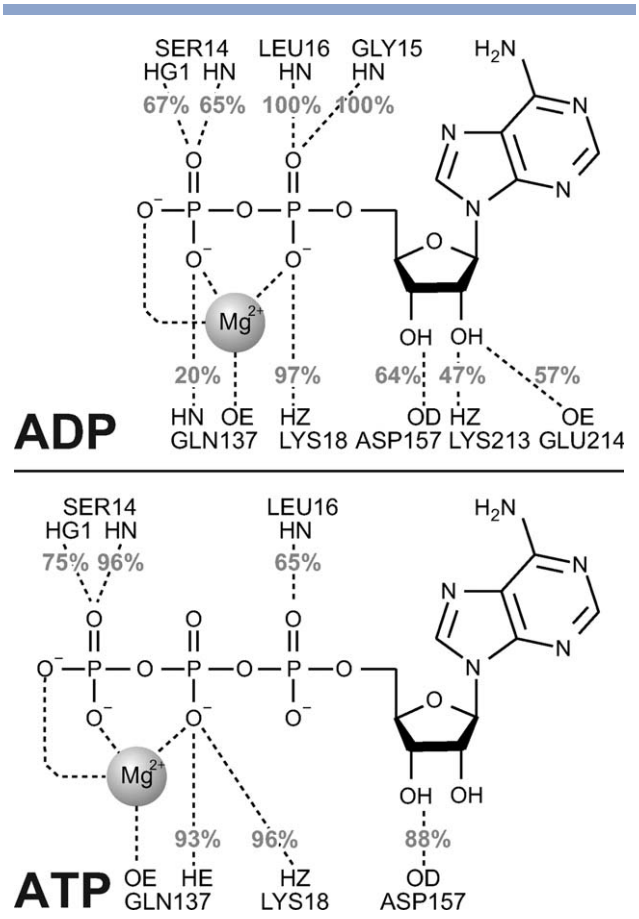

Figure 5

Differences in average nucleotide-binding patterns of actin protomers from the Holmes 2010 ADP- and ATP-filament simulations. Percentages correspond to the fraction of the last 5-ns simulation time the hydrogen bond was formed. Water molecules surrounding the magnesium ion and nucleotide are not shown.

three conformations are apparent. The positions of the sensor loop containing the methylated His73 (residues 70–78; Supporting Information Fig. S3A) and the loop formed by residues 165–170 (Supporting Information Fig. S3C) in the Holmes 2010 model differ from those in the G-actin crystal structure. During the simulation, however, these two loops revert back to the G-actin crystal structure positions again. Supporting Information Figure S3B shows that the twisting of the two lobes of the G-actin structure, that is responsible for the flattening of the protomers in the filament model, is lessened during the simulation. This decrease in flatness of the protomer structure (described by the propeller angle property) was observed in the simulations of the other two filament models (Fig. 2D). In contrast, the slight rotation of subdomain 4 (Supporting Information Fig. S3D) in the Holmes 2010 model is amplified in the MD. The hydrophobic plug slightly changes its position during MD simulation (Supporting Information Fig. S3E) but does not adopt the extended conformation of previous Holmes filament models. This finding is in agreement with a mutational study of the hydrophobic loop that showed that the loop is predominantly in the nonextended position while occasionally exploring other conformations that stabilize or destabilize the filament.[39]

Implications of the nucleotide state

The nucleotide-induced conformational changes of actin and the activation of the ATPase activity on transition from G- to F-actin make the nucleotide binding site critical to understanding the functional cycle of the protein. Hence, the hydrogen-bonding networks between the nucleotide and actin molecule were characterized for each individual protomer. In one of the protomers of the Holmes 2004 model, the ADP molecule left the binding pocket entirely, and in many of the other protomers, the position of the ADP changed significantly by translation or rotation during the simulation. Because of this instability, the nucleotide binding site of the Holmes 2004 simulation was not investigated further. The occupancies of individual hydrogen bonds in the nucleotide binding site of each protomer of the Oda 2009 and Holmes 2010 (ADP and ATP) simulations are shown in Tables S1–3 in the Supporting Information.

A schematic representation of the resulting average hydrogen-bond network of the ADP and ATP forms of the Holmes 2010 filament is given in Figure 5. In agreement with the crystal structures of G-actin, Ser14 forms two hydrogen bonds with the γ-phosphate group in the ATP-bound simulations. However, these shift to the β-phosphate group in the MD of ADP-bound actin. Likewise, the interaction of Lys18 also shifts, from the β-phosphate group in the ATP simulation to the α-phosphate group with ADP. In both simulations (ADP and ATP) of the Holmes 2010 model, Leu16 forms a hydrogen bond with the α-phosphate group and Asp157 interacts with H3T of the adenosine group. Other significant differences include the complete absence of an interaction of Gly15 with the α-phosphate oxygen in the ATP simulation. In G-actin, the HN atoms of Gly15 and Asp157 interact with the oxygen of the β-phosphate group. These two contacts do not occur in the ATP-bound simulation of the Holmes 2010 model.

The most significant difference in the hydrogen bonding patterns between the ATP-bound and ADP-bound systems may concern the hydrogen bond between Gln137 and the oxygen of the β-phosphate, which forms 93% of the time in the ATP-bound case but only 20% of the time for the ADP-bound actin simulation. This interaction was not observed in crystallographic structures of G-actin: in PDB ID 1NWK[40] of ATP-bound G-actin, for example, the distance between Gln137 and the oxygen of the β-phosphate group is 6.7 Å. Gln137 is located at the bottom of the nucleotide-binding cleft, at the hinge

between the two large domains of the actin molecule. As illustrated in Figure S5 in the Supporting Information, the flattening of the G-actin structure during filament formation is responsible for bringing Gln137 closer to the nucleotide, permitting the formation of a stable hydrogen bond during MD simulation of the model. These findings suggest that the repositioning of Gln137 during the G-to-F-actin transition may play a key role in invoking the ATPase activity in F-actin.

DISCUSSION

The resolution of fiber diffraction and EM data used to construct pre-2009 F-actin models was not sufficient to reveal the global conformational change taking place during the G-actin to F-actin transition. However, the higher resolution X-ray data obtained by Oda *et al.*[12] clearly indicate that a twist of the two domains of the U-shaped actin monomer leading to a flattening of the monomer structure is the main global conformational change upon assembly of G-actin to the filament. Oda's finding is supported by a very recent high-resolution EM study.[15] This global change is incorporated in both the present Holmes 2010 model and that of Oda 2009. Although the two models exhibit similar low-resolution structures they differ significantly in their details. In Oda 2009, adjustments of the local structure were made so as to reduce the *R*-factor. However, in the present model, these adjustments have been avoided thus preserving the stereochemistry and keeping the local structure as close as possible to that of the crystallographic G-actin.

Internal dynamics in actin filaments extends over timescales at least to the second.[41] Hence the 30 ns of MD simulations carried out here is orders of magnitude shorter than would be required for a full exploration of the configurational space of the system. However, MD does allow a local free energy search around the modeled conformation of the native state. Local structural processes with relatively fast relaxation times, such as, for example, short-range hydrogen-bond formation, will converge, and this is seen in the results presented here.

The progression in quality of the three structural models examined is apparent on subjecting them to MD simulation. Among the three tested models, the structural stability of Holmes 2004 is the lowest: the average RMSD of the protomers and the structural variation among the 13 protomers are both significantly higher than for the other two models. Both in the initial model and during the MD simulation, the distance between the filament strands is the highest. Further, all protomers in Holmes 2004 show unfolding of some of the secondary structural elements. In the majority of protomers, the ADP is unstable within the nucleotide binding site and even leaves the binding pocket entirely in one of the protomers.

The relative structural instability of the Holmes 2004 model may be partly due to the quality of the experimental diffraction data and partly due to the way the structure had to be generated: the experimental data were not sufficiently detailed to permit structural change within the four subdomains, and so, the model was built by treating the G-actin subdomains as independent rigid bodies, adjusting their positions during the fitting. No side chain optimization at the interface between protomers within the filament was performed.

In comparison with Holmes 2004, the simulations of the Oda 2009 and Holmes 2010 filaments exhibit higher structural stability, and their observed properties are closer to the expected values. The higher structural stability of the Oda 2009 model in comparison with another older model was also found in a recent MD study.[42] The average RMSD of the Oda 2009 and Holmes 2010 model protomers is very close to that of the simulation of the G-actin crystal structure. In contrast, the propeller angle formed by the four subunits of the actin molecule is much higher in the G-actin simulation than in the simulations of the F-actin models. This is to be expected, as the major conformational transition that occurs on incorporation of G-actin into the filament is believed to be a twist of the actin molecule that flattens the structure and significantly reduces the size of the cleft between the two domains.[12,36] However, in all three simulations of F-actin models, the initially very small propeller angle of 2–3° increases significantly to about 7–9°, while still remaining well below the 22° of the G-actin simulation. The fact that all three models show this same trend may indicate that the flattening twist of the actin molecule imposed during model building is slightly too high. In the simulation of Oda 2009, the increase of the propeller angle during MD is steady but slower than that of the other two models. This may arise from the fact that the interprotomer interface was optimized in the Oda model but not in the two Holmes models, resulting in a higher number of nonbonded interactions between protomers within the filament (Fig. 2C) and thus stabilizing the interprotomer interface and delaying the propeller angle increase over the simulation time. In contrast to the interactions between protomers, the number of hydrogen bonds within the actin molecules is significantly lower throughout the simulation of the Oda 2009 model than in G-actin of Holmes 2010. An explanation for this difference may again be in the different approach that was taken to build the two models. As part of the model refinement process, Oda *et al.* used a simulated annealing procedure to minimize the R-factor. As a result, hydrogen bonds within the actin molecule were disrupted. In contrast, the straightforward modeling procedure exercised here aimed at avoiding disruption of native nonbonded contacts within the protomers: The Holmes 2010 model is essentially the crystallographic structure of G-actin with a twist into a more planar form, carried out with as

little impact on the intraprotomer interactions as possible. Indeed, the average hydrogen-bond count in the simulation of the Holmes 2010 model is even slightly higher than that of the crystallographic G-actin structure, consistent with the more open structure of the G-actin monomer.

Experimental studies suggest that the conformation of ADP- and ATP-F-actin must differ, as global properties such as the persistence length or the binding affinity of some actin-binding proteins depend on the nucleotide state of the filament. The structural differences between simulations of the ADP- and ATP-bound Holmes 2010 model observed here are relatively small. Longer simulation times than are currently possible are likely to be necessary to fully observe the conformational changes between the two states of the filament. Hence, we focus here on the local differences in the nucleotide binding pocket, from which potential global conformational differences of the protomer will originate. Although the initial protein structures were identical, we found that in MD simulation the nucleotide-binding pocket of the ADP- and ATP-bound Holmes 2010 filaments differ significantly from each other. Furthermore, differences also exist between the ATP-binding patterns of the G-actin X-ray structure and the average ATP-bound F-actin protomer, as would be expected as, in contrast to G-actin, F-actin does exhibit significant ATPase activity.

Several studies have investigated possible mechanisms of hydrolysis of ATP in actin.[43–46] A study of actin mutants revealed the significance of Gln137 for filament polymerization and cleavage of the γ-phosphate group: replacing this glutamine with an alanine caused a fourfold slowdown of ATP hydrolysis.[45] Further, in Ref. 45, it was suggested that the twist of the ATP-bound actin monomer upon integration into the filament leads to relocation of Gln137 bringing it in close proximity to ATP.[12] In agreement with another recent MD study of the actin filament,[42] the present simulations support this hypothesis. Unlike in the crystal structures of G-actin or the simulation of the ADP-bound Holmes 2010 model, Gln137 is close to the ATP in the MD of the Holmes 2010 model, forming a stable hydrogen bond with the oxygen atom of the β-phosphate group and may therefore play a direct role in hydrolysis. However, a very recent EM-based reconstruction of the nucleotide-binding site in the actin filament suggests the role of Gln137 for ATPase activity to be indirect[46] and hence uncertainty in the role of Gln137 remains.

The present F-actin model possesses both a global conformation in agreement with the recent model of Ref. 12 and a consistent intraprotomer stereochemistry. However, it is unlikely to be the last word on the subject and intense recent experimental and simulation activity means that the situation appears to be fast approaching whereby definitive atomic-detail descriptions of the filament in biologically functional states will be obtained. At that point, simulation will again be needed to characterize the hydrolysis reaction mechanism in detail and its coupling to conformational pathways between the functional states.

ACKNOWLEDGMENTS

The authors thank Isabella Daidone and Michael Lorenz for helpful discussion. The majority of the computations were performed on the Jaguar Cray XT4 supercomputer at the National Center for Computational Sciences at Oak Ridge National Lab.

REFERENCES

1. Lodish H, Berk A, Zipursky SL, Matsudaira P, Baltimore D, Darnell J. Molecular cell biology. W. H. Freeman; New York, 1999. 1184 p.
2. Selby CC, Bear RS. The structure of actin-rich filaments of muscles according to x-ray diffraction. J Biophys Biochem Cytol 1956;2:71–85.
3. Oosawa F, Kasai M. A theory of linear and helical aggregations of macromolecules. J Mol Biol 1962;4:10–21.
4. Egelman EH, Francis N, DeRosier DJ. F-actin is a helix with a random variable twist. Nature 1982;298:131–135.
5. Astbury WT, Perry SV, Reed R, Spark LC. An electron microscopy and X-ray study of actin. Biochim Biophys Acta 1947;1:379–392.
6. Cohen C, Hansen J. An X-ray diffraction study of F-actin. Biochim Biophys Acta 1956;21:177–178.
7. Hanson J, Lowy J. The structure of F-actin of actin filaments isolated from muscle. J Mol Biol 1963;6:46–60.
8. Trinick J, Cooper J, Seymour J, Egelman EH. Cryo-electron microscopy and three-dimensional reconstruction of actin filament. J Microsc 1986;141:349–360.
9. Kabsch W, Mannherz HG, Suck D, Pai EF, Holmes KC. Atomic structure of the actin:DNase I complex. Nature 1990;347:37–44.
10. Holmes KC, Popp D, Gebhard W, Kabsch W. Atomic model of the actin filament. Nature 1990;347:44–49.
11. Holmes KC, Schröder RR, Sweeney HL, Houdusse A. The structure of the rigor complex and its implications for the power stroke. Philos Trans R Soc Lond B Biol Sci 2004;359:1819–1828.
12. Oda T, Iwasa M, Aihara T, Maeda Y, Narita A. The nature of the globular- to fibrous-actin transition. Nature 2009;457:441–445.
13. Lorenz M, Popp D, Holmes KC. Refinement of the F-actin model against X-ray fiber diffraction data by the use of a directed mutation algorithm. J Mol Biol 1993;234:826–836.
14. Tirion MM, ben-Avraham D, Lorenz M, Holmes KC. Normal modes as refinement parameters for the f-actin model. Biophys J 1995;68:5–12.
15. Fujii T, Iwane AH, Yanagida T, Namba K. Direct visualization of secondary structures of F-actin by electron cryomicroscopy. Nature 2010;467:724–728.
16. Oda T, Makino K, Yamashita I, Namba K, Maeda Y. The helical parameters of F-actin precisely determined from X-ray fiber diffraction of well-oriented sols. Results Probl Cell Differ 2001;32:43–58.
17. Isambert H, Venier P, Maggs AC, Fattoum A, Kassab R, Pantaloni D, Carlier MF. Flexibility of actin filaments derived from thermal fluctuations. Effect of bound nucleotide, phalloidin, and muscle regulatory proteins. J Biol Chem 1995;270:11437–11444.
18. Pollard TD, Borisy GG. Cellular motility driven by assembly and disassembly of actin filaments. Cell 2003;112:453–465.
19. Otterbein LR, Graceffa P, Dominguez R. The crystal structure of uncomplexed actin in the ADP state. Science 2001;293:708–711.
20. Berman HM, Westbrook J, Feng Z, Gilliland G, Bhat TN, Weissig H, Shindyalov IN, Bourne PE. The Protein Data Bank. Nucleic Acids Res 2000;28:235–242.

21. Sablin EP, Dawson JF, VanLoock MS, Spudich JA, Egelman EH, Fletterick RJ. How does ATP hydrolysis control actin's associations? Proc Nat Acad Sci USA 2002;99:10945–10947.
22. Holmes KC, Angert I, Kull FJ, Jahn W, Schroder RR. Electron cryo-microscopy shows how strong binding of myosin to actin releases nucleotide. Nature 2003;425:423–427.
23. Gordon JC, Myers JB, Folta T, Shoja V, Heath LS, Onufriev A. H++: a server for estimating pKas and adding missing hydrogens to macromolecules. Nucleic Acids Res 2005;33(Web Server issue): W368–W371.
24. Yao X, Grade S, Wriggers W, Rubenstein PA. His(73), often methylated, is an important structural determinant for actin. A mutagenic analysis of HIS(73) of yeast actin. J Biol Chem 1999;274:37443–37449.
25. Estes JE, Selden LA, Kinosian HJ, Gershman LC. Tightly-bound divalent cation of actin. J Muscle Res Cell Motil 1992;13:272–284.
26. Phillips JC, Braun R, Wang W, Gumbart J, Tajkhorshid E, Villa E, Chipot C, Skeel RD, Kale L, Schulten K. Scalable molecular dynamics with NAMD. J Comput Chem 2005;26:1781–1802.
27. MacKerell AD, Bashford D, Bellott M, Dunbrack RL, Evanseck JD, Field MJ, Fischer S, Gao J, Guo H, Ha S, Joseph-McCarthy D, Kuchnir L, Kuczera K, Lau FTK, Mattos C, Michnick S, Ngo T, Nguyen DT, Prodhom B, Reiher WE, Roux B, Schlenkrich M, Smith JC, Stote R, Straub J, Watanabe M, Wiorkiewicz-Kuczera J, Yin D, Karplus M. All-atom empirical potential for molecular modeling and dynamics studies of proteins. J Phys Chem B 1998; 102:3586–3616.
28. Jorgensen WLCJ, Madura J D, Impey R W, Klein M L. Comparison of simple potential functions for simulating liquid water. J Chem Phys 1983;79:926–935.
29. Darden T, York D, Pedersen L. Particle mesh Ewald: an Nlog(N) method for Ewald sums in large systems. J Chem Phys 1993;98: 10089–10092.
30. Evans DJ, Holian BL. The Nose-Hoover thermostat. J Chem Phys 1985;83:4069–4074.
31. DeLano WL. The PyMOL molecular graphics system. Version 1.3, Schrödinger, LLC. Palo Alto, CA, USA; 2002.
32. Cong Y, Topf M, Sali A, Matsudaira P, Dougherty M, Chiu W, Schmid MF. Crystallographic conformers of actin in a biologically active bundle of filaments. J Mol Biol 2008;375:331–336.
33. Oztug Durer ZA, Diraviyam K, Sept D, Kudryashov DS, Reisler E. F-actin structure destabilization and DNase I binding loop: fluctuations mutational cross-linking and electron microscopy analysis of loop states and effects on F-actin. J Mol Biol 2010;395:544–557.
34. Chu J-W, Voth GA. Allostery of actin filaments: molecular dynamics simulations and coarse-grained analysis. Proc Nat Acad Sci USA 2005;102:13111–13116.
35. Pfaendtner J, Branduardi D, Parrinello M, Pollard TD, Voth GA. Nucleotide-dependent conformational states of actin. Proc Natl Acad Sci USA 2009;106:12723–12728.
36. Splettstoesser T, Noe F, Oda T, Smith JC. Nucleotide-dependence of G-actin conformation from multiple molecular dynamics simulations and observation of a putatively polymerization-competent superclosed state. Proteins 2009;76:353–364.
37. Dalhaimer P, Pollard TD, Nolen BJ. Nucleotide-mediated conformational changes of monomeric actin and Arp3 studied by molecular dynamics simulations. J Mol Biol 2008;376:166–183.
38. Shvetsov A, Stamm JD, Phillips M, Warshaviak D, Altenbach C, Rubenstein PA, Hideg K, Hubbell WL, Reisler E. Conformational dynamics of loop 262–274 in G- and F-actin. Biochemistry 2006; 45:6541–6549.
39. Scoville D, Stamm J, Toledo-Warshaviak D, Altenbach C, Phillips M, Shvetsov A, Rubenstein P, Hubbell W, Reisler E. Hydrophobic Loop Dynamics and Actin Filament Stability. Biochemistry 2006;45: 13576–13584.
40. Graceffa P, Dominguez R. Crystal structure of monomeric actin in the ATP state. Structural basis of nucleotide-dependent actin dynamics. J Biol Chem 2003;278:34172–34180.
41. Kozuka J, Yokota H, Arai Y, Ishii Y, Yanagida T. Dynamic polymorphism of single actin molecules in the actin filament. Nat Chem Biol 2006;2:83–86.
42. Pfaendtner J, Lyman E, Pollard TD, Voth GA. Structure and Dynamics of the Actin Filament. J Mol Biol 2009;396:252–263.
43. Vorobiev S, Strokopytov B, Drubin DG, Frieden C, Ono S, Condeelis J, Rubenstein PA, Almo SC. The structure of nonvertebrate actin: implications for the ATP hydrolytic mechanism. Proc Nat Acad Sci USA 2003;100:5760–5765.
44. Akola J, Jones RO. Density functional calculations of ATP systems. 2. ATP hydrolysis at the active site of actin. J Phys Chem B 2006; 110:8121–8129.
45. Iwasa M, Maeda K, Narita A, Maeda Y, Oda T. Dual roles of Gln137 of actin revealed by recombinant human cardiac muscle alpha-actin mutants. J Biol Chem 2008;283:21045–21053.
46. Murakami K, Yasunaga T, Noguchi TQ, Gomibuchi Y, Ngo KX, Uyeda TQ, Wakabayashi T. Structural basis for actin assembly, activation of ATP hydrolysis, and delayed phosphate release. Cell 2010; 143:275–287.